Cell Reports, Volume *24*

Supplemental Information

Regulation of KIF1A-Driven Dense Core Vesicle Transport: Ca^{2+}/CaM Controls DCV Binding and Liprin-α/TANC2 Recruits DCVs to Postsynaptic Sites

Riccardo Stucchi, Gabriela Plucińska, Jessica J.A. Hummel, Eitan E. Zahavi, Irune Guerra San Juan, Oleg Klykov, Richard A. Scheltema, A.F. Maarten Altelaar, and Casper C. Hoogenraad

SUPPLEMENTAL FIGURES

Figure S1

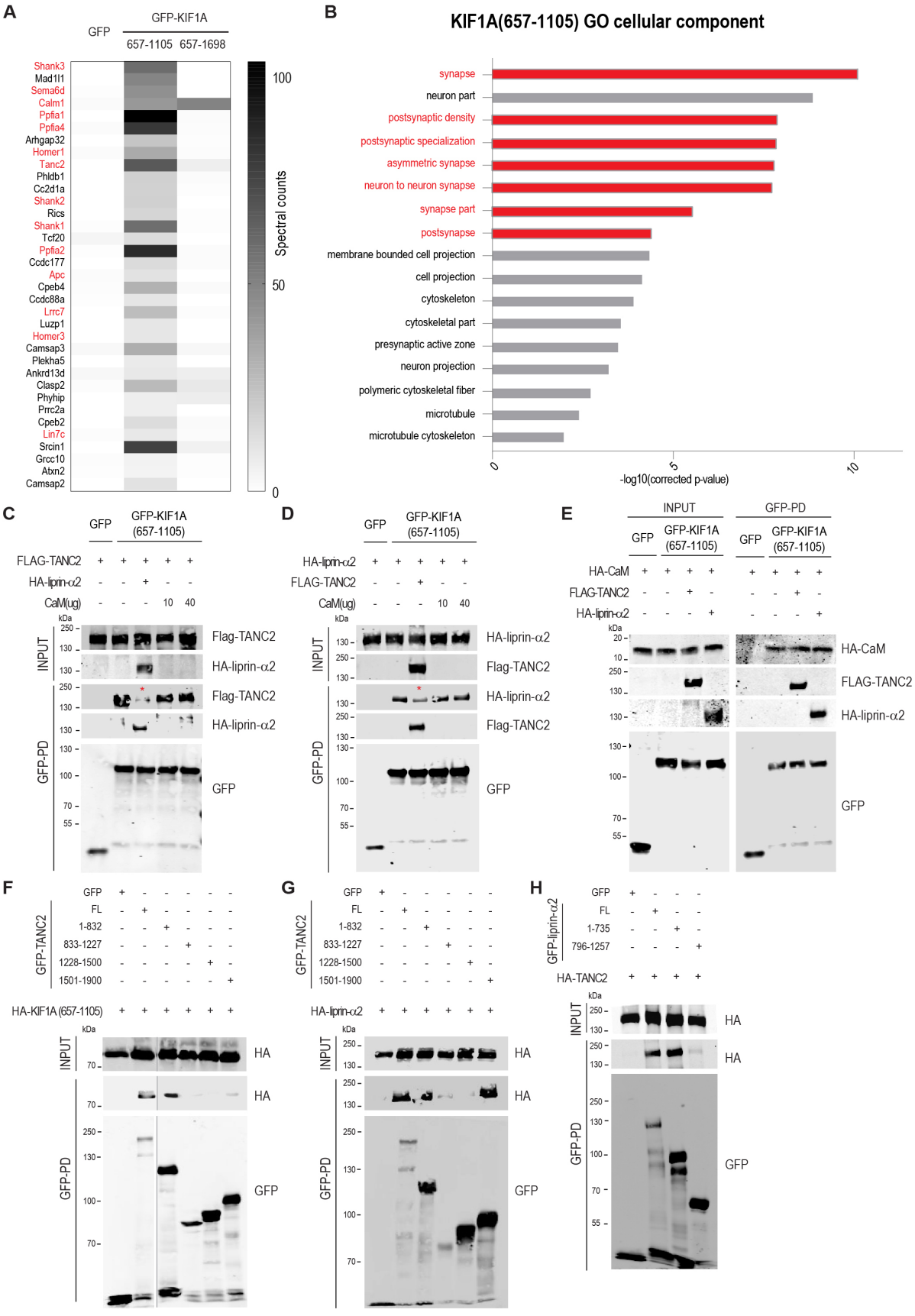
A
GFP
GFP-KIF1A
657-1105
657-1698
Shank3
Mad1l1
Sema6d
Calm1
Ppfia1
Ppfia4
Arhgap32
Homer1
Tanc2
Phldb1
Cc2d1a
Shank2
Rics
Shank1
Tcf20
Ppfia2
Ccdc177
Apc
Cpeb4
Ccdc88a
Lrrc7
Luzp1
Homer3
Camsap3
Plekha5
Ankrd13d
Clasp2
Phyhip
Prrc2a
Cpeb2
Lin7c
Srcin1
Grcc10
Atxn2
Camsap2
100
Spectral counts
50
0
B
KIF1A(657-1105) GO cellular component
synapse
neuron part
postsynaptic density
postsynaptic specialization
asymmetric synapse
neuron to neuron synapse
synapse part
postsynapse
membrane bounded cell projection
cell projection
cytoskeleton
cytoskeletal part
presynaptic active zone
neuron projection
polymeric cytoskeletal fiber
microtubule
microtubule cytoskeleton
0
5
10
-log10(corrected p-value)
C
GFP
GFP-KIF1A (657-1105)
FLAG-TANC2
HA-liprin-α2
CaM(ug)
10
40
kDa
INPUT
GFP-PD
Flag-TANC2
HA-liprin-α2
GFP
D
GFP
GFP-KIF1A (657-1105)
HA-liprin-α2
FLAG-TANC2
CaM(ug)
10
40
kDa
INPUT
GFP-PD
HA-liprin-α2
Flag-TANC2
GFP
E
INPUT
GFP-PD
GFP
GFP-KIF1A (657-1105)
HA-CaM
FLAG-TANC2
HA-liprin-α2
kDa
GFP
F
GFP-TANC2
GFP
FL
1-832
833-1227
1228-1500
1501-1900
HA-KIF1A (657-1105)
kDa
INPUT
GFP-PD
HA
GFP
G
GFP-TANC2
GFP
FL
1-832
833-1227
1228-1500
1501-1900
HA-liprin-α2
kDa
INPUT
GFP-PD
HA
GFP
H
GFP-liprin-α2
GFP
FL
1-735
796-1257
HA-TANC2
kDa
INPUT
GFP-PD
HA
GFP

Figure S1. Related to Figure 1. KIF1A(657-1105) interacts with TANC2, liprin-α2, CaM and shows high binding affinity for a restricted group of post synaptic density (PSD) proteins

(A) List of KIF1A (657-1105) interactors identified by LC/MS-MS in rat brain affinity purification (AP) experiments. BioGFP-CTR and bioGFP-KIF1A truncated isoforms (657-1105; 657-1698) were firstly expressed in HEK293 cells, purified using streptavidin-pulldowns and then incubated with rat brain extracts. Candidate proteins identified by MS are considered true KIF1A(657-1105) interactors when their probability >0.98 using the SAINT algorithm. Heat map shows total spectral counts detected for each protein candidate in AP-MS experiments of bioGFP, bioGFP-KIF1A(657-1105) or bioGFP-KIF1A(657-1698). Selected candidates shown in the graph are neuronal specific interacting partners not detected in a control bio-GFP-KIF1A(657-1105) AP-MS experiment performed in HEK293 cells. See also Table S1.

(B) Gene ontology analysis (cellular component) of KIF1A(657-1105) interacting proteins (P-value>0.98). See also Figure S1A and Table S1.

(C) bioGFP-KIF1A(657-1105) was expressed in HEK293 cells, purified using streptavidin-pulldowns and incubated with protein extracts of cells expressing FLAG-TANC2 alone, or in combination with extracts of cells expressing HA-liprin-α2 or in combination with 10 or 40 μg of purified calmodulin (Sigma). Western blot detection was performed using FLAG, HA and GFP antibodies.

(D) bioGFP-KIF1A(657-1105) was expressed in HEK293 cells, purified and incubated with protein extracts of cells expressing HA-liprin-α2 alone, or in combination with extracts of cells expressing FLAG-TANC2 or in combination with 10 or 40 ug of purified calmodulin (Sigma). Western blot detection was performed using HA, FLAG and GFP antibodies.

(E) bioGFP-KIF1A(657-1105) was expressed in HEK293 cells, purified using streptavidin-pulldowns and incubated with protein extracts of cells expressing HA-CaM alone, or in combination with extracts of cells expressing FLAG-TANC2 or in combination with extracts of cells expressing HA-liprin-α2. Western blot detection was performed using HA, FLAG and GFP antibodies.

(F) Western blots of HA-KIF1A(657-1105) in AP experiments of full length GFP-TANC2 and GFP-TANC2 fragments (1-832, 833-1227, 1228-1500, 1501-1900) from co-transfected HEK293 cells.

(G) Western blots of HA-liprin-α2 in AP experiments of GFP, full length GFP-TANC2, or GFP-TANC2 fragments (1-832, 833-1227, 1228-1500, 1501-1900).

(H) Western blots of HA-TANC2 in AP experiments of GFP, full length GFP-liprin-α2, GFP-liprin-α2(1–735) or GFP-liprin-α2(796–1257).

Figure S2

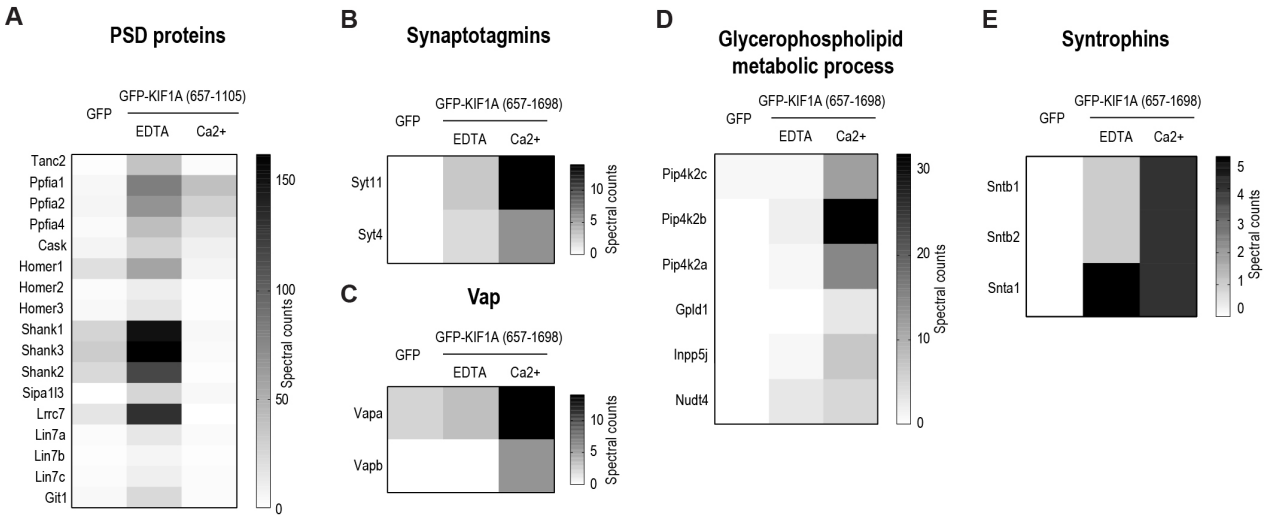

Figure S2. Related to Figure 3. KIF1A interactome is modulated by calcium

(A) BioGFP-KIF1A(657-1105) was incubated with rat brain extracts in presence of 2mM EDTA or 2mM Ca^{2+}. Heat map shows selected post synaptic density (PSD) proteins co-purified with KIF1A(657-1105)_EDTA and identified by MS. Relative abundance of each protein is represented as total spectral counts detected in bioGFP (ctr), bioGFP-KIF1A(657-1105)_EDTA or bioGFP-KIF1A(657-1105)_Ca^{2+}.

(B-E) BioGFP-KIF1A(657-1698) was incubated with rat brain extracts in presence of 2mM EDTA or 2mM Ca^{2+}. Relative abundance of each protein is represented as total spectral counts detected in bioGFP (ctr), bioGFP-KIF1A(657-1698)_EDTA or bioGFP-KIF1A(657-1698)_Ca^{2+}. Heat maps show selected co-purified proteins with KIF1A(657-1698)_Ca^{2+}: Synaptotagmin4 (Syt4) and synaptotagmin11 (Syt11) (B); Vapa and Vapb(C); phosphatidylinositol 5-phosphate 4-kinase (Pip4k2), phosphatidylinositol-glycan-specific phospholipase D (Gpld1), inositol polyphosphate 5-phosphatase (Inpp5), diphosphoinositol polyphosphate phosphohydrolase 2 (Nudt4) (D); syntrophins (Snt) (E).

Figure S3

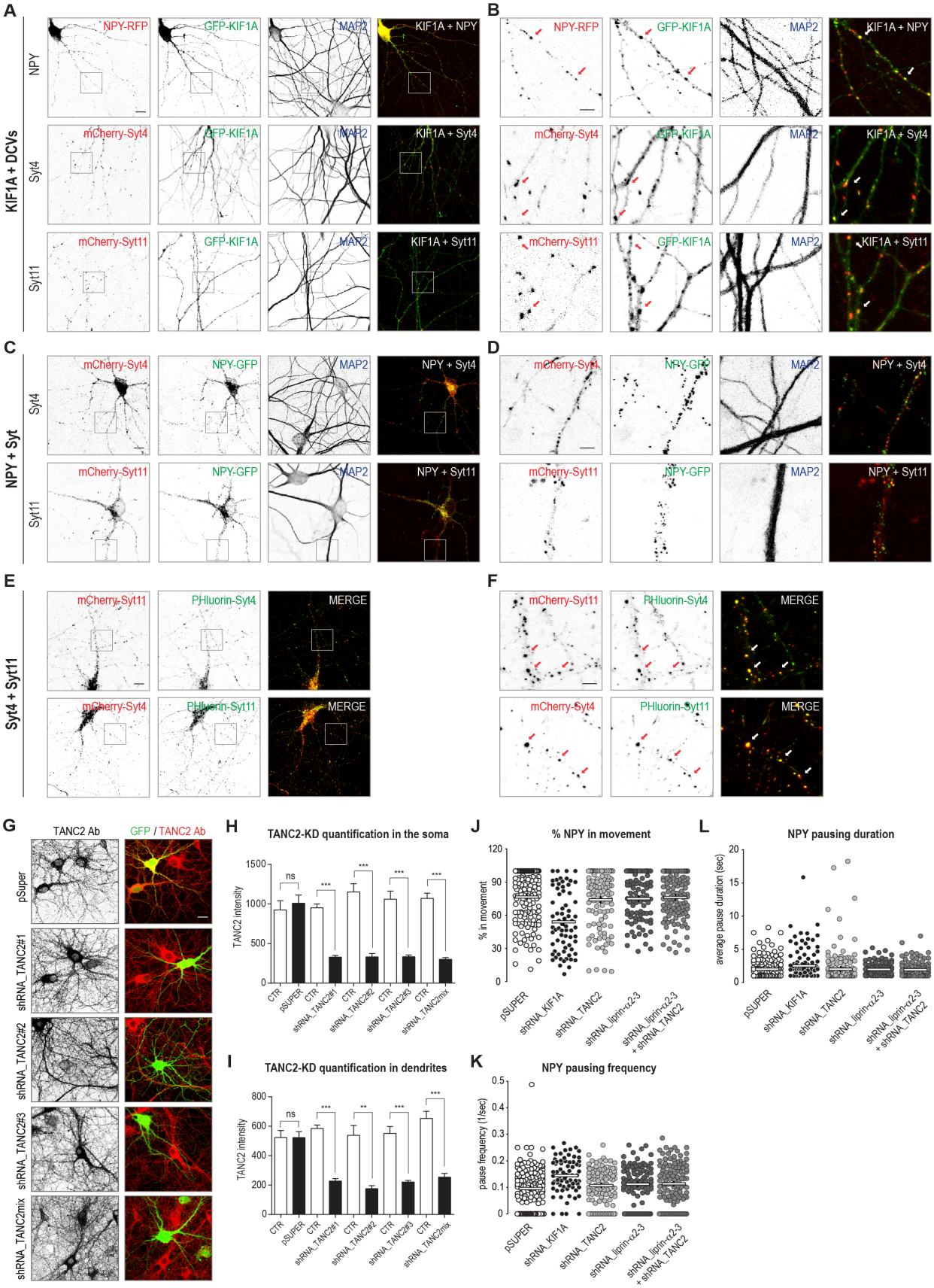
A
B
KIF1A + DCVs
NPY
Syt4
Syt11
NPY-RFP
GFP-KIF1A
MAP2
KIF1A + NPY
mCherry-Syt4
KIF1A + Syt4
mCherry-Syt11
KIF1A + Syt11
C
D
NPY + Syt
NPY-GFP
NPY + Syt4
NPY + Syt11
E
F
Syt4 + Syt11
PHluorin-Syt4
PHluorin-Syt11
MERGE
G
TANC2 Ab
GFP / TANC2 Ab
pSuper
shRNA_TANC2#1
shRNA_TANC2#2
shRNA_TANC2#3
shRNA_TANC2mix
H
TANC2-KD quantification in the soma
TANC2 intensity
ns
I
TANC2-KD quantification in dendrites
J
% NPY in movement
% in movement
pSUPER
shRNA_KIF1A
shRNA_TANC2
shRNA_liprin-α2-3
shRNA_liprin-α2-3 + shRNA_TANC2
K
NPY pausing frequency
pause frequency (1/sec)
L
NPY pausing duration
average pause duration (sec)

Figure S3. Related to Figure 5. KIF1A transports DCVs in dendrites but DCV motility is not influenced by TANC2 and liprin-α

(A) Representative images of rat hippocampal neurons (DIV11-DIV14) co-transfected with GFP-KIF1A (green) in combination with NPY-RFP (red), mCherry-Syt4 (red) or mCherry-Syt11 (red) and stained for MAP2 (blue). Scale bar, 10μm.

(B) Images correspond to higher magnifications of the selected areas highlighted in the nearby figures. Arrows point to co-localizing puncta. Scale bar, 5μm.

(C) Neurons co-transfected with NPY-GFP (green) in combination with mCherry-Syt4 (red) or mCherry-Syt11 (red) and stained for MAP2 (blue). Scale bar, 10μm.

(D) Images correspond to higher magnifications of the selected areas highlighted in the nearby figures. Scale bar, 5μm.

(E) Neurons co-transfected with Phluorin-Syt4 (green) in combination with mCherry-Syt11 (red), or with Phluorin-Syt11 (green) in combination with mCherry-Syt4 (red). Scale bar, 10μm.

(F) Images correspond to higher magnifications of the selected areas highlighted in the nearby figures. Arrows point to co-localizing puncta. Scale bar, 5μm.

(G) Representative images of hippocampal neurons (DIV11-14) knockdown for TANC2 with indicated shRNA constructs (shRNA_TANC2#1, shRNA_TANC2#2, shRNA_TANC2#3, shRNA_TANC2mix), filled with GFP (green) and stained with TANC2 polyclonal antibody (red). Scale bar, 20μm.

(H-I) Quantifications of TANC2 fluorescent-staining intensities in KD-neurons shown in Figure S3G. (H) TANC2 staining intensity in the soma of transfected KD-neurons is compared to TANC2 intensity in the soma of non-transfected neurons within the same images; (I) TANC2 staining intensity in neurites of transfected KD-neurons is compared to TANC2 intensity in neurites of non-transfected neurons within the same images. The bars show mean ± s.e.m. (n=9-13 neurons (H), n=27-39 neurites (I); $^{**}P<0.01$, *paired t*-test; $^{***}P<0.001$, *paired t*-test).

(J-L) Quantifications of NPY trafficking parameters in dendrites of neurons (DIV11-14) co-transfected with NPY-GFP in combination with pSuper, shRNA_KIF1A, shRNA_TANC2, shRNA_liprin-α2–3, sh_RNA_liprin-2-3 + sh_RNA_TANC2; percentage of NPY vesicles in movement (J), NPY pause frequency (K), NPY average pause duration (L). Bars show the mean; (n=17-58 dendrites).

Figure S4

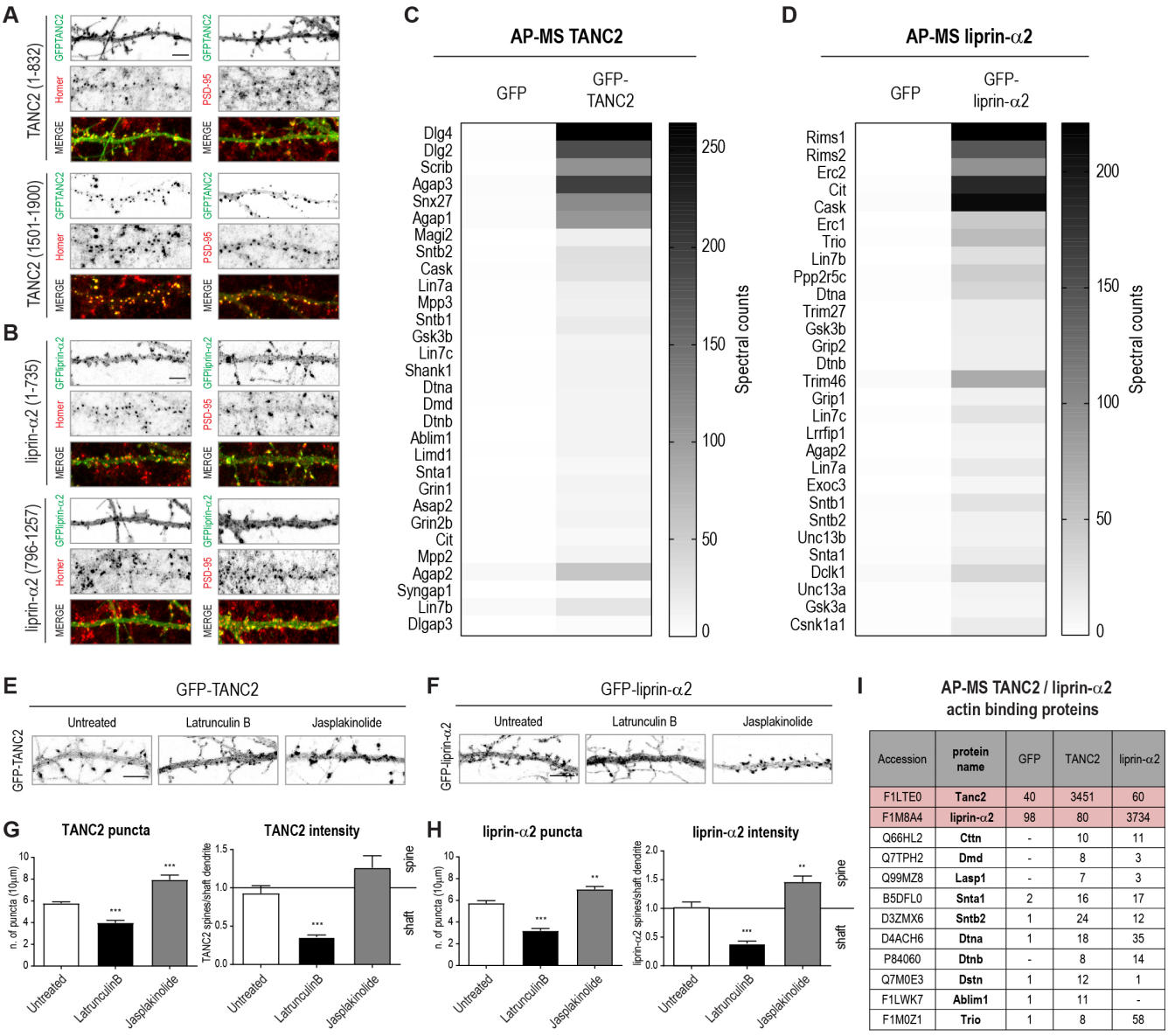

I AP-MS TANC2 / liprin-α2 actin binding proteins

Accession	protein name	GFP	TANC2	liprin-α2
F1LTE0	**Tanc2**	40	3451	60
F1M8A4	**liprin-α2**	98	80	3734
Q66HL2	**Cttn**	-	10	11
Q7TPH2	**Dmd**	-	8	3
Q99MZ8	**Lasp1**	-	7	3
B5DFL0	**Snta1**	2	16	17
D3ZMX6	**Sntb2**	1	24	12
D4ACH6	**Dtna**	1	18	35
P84060	**Dtnb**	-	8	14
Q7M0E3	**Dstn**	1	12	1
F1LWK7	**Ablim1**	1	11	-
F1M0Z1	**Trio**	1	8	58

Figure S4. Related to Figure 6. TANC2 and liprin-α2 are scaffolding proteins in the post synaptic density (PSD)

(A) Representative dendritic protrusions of neurons (DIV14-17) expressing GFP-TANC2 n-terminal (1-832) or GFP-TANC2 c-terminal fragment (1501-1900) and stained for the post-synaptic proteins Homer or PSD-95 (red). Scale bar, 5μm.

(B) Representative dendritic protrusions of neurons (DIV14-17) expressing GFP-liprin-α2 n-terminal (1-735) or GFP-liprin-α2 c-terminal fragment (796-1257) and stained for the post-synaptic proteins Homer or PSD-95 (red). Scale bar, 5μm.

(C) List of significant TANC2 interactors identified by MS in AP experiments using bioGFP-TANC2 as bait. BioGFP-CTR and bioGFP-TANC2 were expressed in HEK293 cells, purified using streptavidin-pulldowns and then incubated with rat brain extracts. Co-purified proteins have been identified by AP-MS and have been classified as TANC2 interactors if

probability >0.90 using the SAINT algorithm. Heat map shows total spectral counts in bioGFP-CTR and bioGFP-TANC2. See also Table S3.

(D) List of significant liprin-α2 interactors identified by LC/MS-MS in AP experiments using bioGFP-liprin-α2 as bait. BioGFP-CTR and bioGFP-liprin-α2 were purified using streptavidin-pulldowns and then incubated with rat brain extracts. Co-purified proteins have been identified by AP-MS and have been classified as putative liprin-α2 interactors if probability >0.90 using the SAINT algorithm. Heat map shows total spectral counts in bioGFP-CTR and bioGFP-liprin-α2. See also Table S4.

(E) Dendritic protrusions of neurons (DIV14-17) expressing GFP-TANC2 and treated with DMSO (Untreated), LatrunculinB or Jasplakinolide for 1h. Scale bar, 5μm.

(F) Dendritic protrusions of neurons (DIV14-17) expressing GFP-liprin-α2 and treated with DMSO (Untreated), LatrunculinB or Jasplakinolide for 1h. Scale bar, 5μm.

(G) Quantifications of total GFP-TANC2 puncta in dendrites (left panel) and of TANC2 intensity in spines/dendritic shaft (right panel) in DMSO (Untreated), Latrunculin B or Jasplakinolide treated neurons (Figure S4E). The bars show mean ± s.e.m. (n=27-30 dendrites; $^{***}P<0.001$, *t*-test).

(H) Quantifications of total GFP-liprin-α2 puncta in dendrites (left panel) and of liprin-α2 intensity in spines/dendritic shaft (right panel) in DMSO (Untreated), Latrunculin B or Jasplakinolide treated neurons (Figure S4F). The bars show mean ± s.e.m. (n=24-31 dendrites, $^{**}P<0.01$, *t*-test, $^{***}P<0.001$, *t*-test).

(I) Table represents selected actin binding proteins co-purified with bioGFP-TANC2 or bioGFP-liprin-α2 and identified by MS (Cttn=Cortactin, Dmd=Dystrophin, Lasp1=LIM and SH3 domain protein 1, Snt=Syntrophin, Dtn=Dystrobrevin, Dstn=Destrin, Ablim=Actin-binding LIM protein, Trio=Triple functional domain protein). Relative abundance of each protein is represented as total spectral counts. See also Table S3-4.

Figure S5

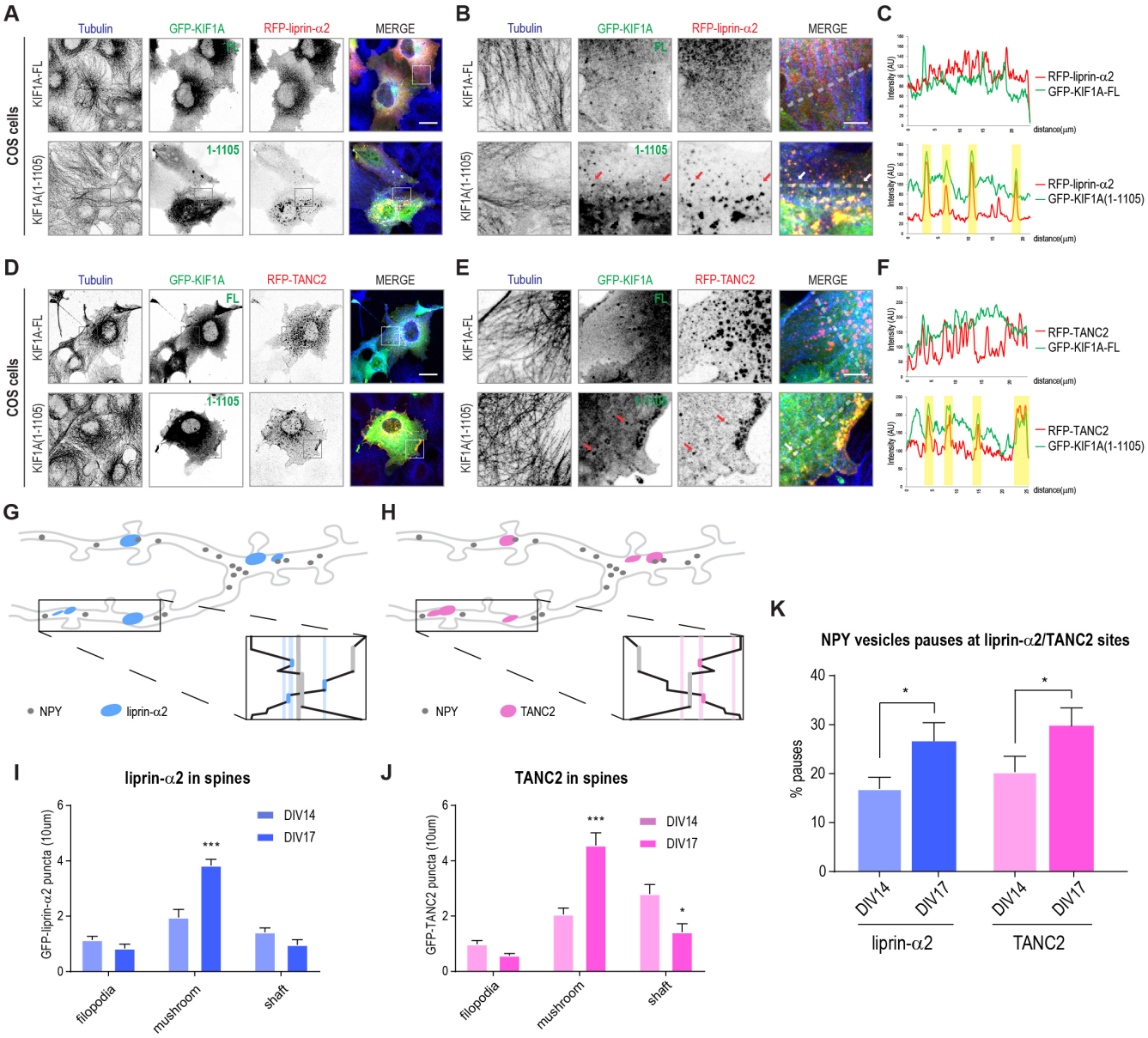

Figure S5. Related to Figure 7. TANC2 and liprin-α2 act as synaptic signposts tethering KIF1A-transported DCVs

(A) Representative images of COS7 cells co-transfected with GFP-KIF1A_full length or GFP-KIF1A(1-1105) (green) in combination with RFP-liprin-α2 (red) and stained for α-tubulin (blue). Scale bar, 20μm.

(B) Images correspond to higher magnifications of the selected areas highlighted in the nearby figures. Arrows point to co-localizing puncta. Scale bar, 5μm.

(C) Line scans of fluorescence intensity of GFP-KIF1A and RFP-liprin-α2 in Figure S5B along the transparent white line.

(D) Representative images of COS7 cells co-transfected with GFP-KIF1A_full length or GFP-KIF1A(1-1105) (green) in combination with RFP-TANC2 (red) and stained for α-tubulin (blue). Scale bar, 20μm.

(E) Images correspond to higher magnifications of the selected areas highlighted in the nearby figures. Arrows point to co-localizing puncta. Scale bar, 5μm.

(F) Line scans of fluorescence intensity of GFP-KIF1A and RFP-TANC2 in Figure S5E along the transparent white line.

(G-H) Graphical representation of NPY vesicles pausing at liprin-α2 (G) or TANC2 (H) static synaptic clusters.

(I-J) Quantifications of GFP-liprin-α2 (I) or GFP-TANC2 (J) puncta in filopodia, mushroom spines or dendritic shaft in DIV14/DIV17 neurons. The bars show mean ± s.e.m. (n=31-63 dendrites; $^{*}P<0.05$, *t*-test, $^{***}P<0.001$, *t*-test).

(K) Quantifications of percentage of NPY vesicles pauses at liprin-α2/TANC2 immobile clusters calculated on the total amount of NPY vesicles pauses, in DIV14/DIV17 neurons. The bars show mean ± s.e.m. (n=15-31 dendrites, $^{*}P<0.05$, *t*-test).

Figure S6

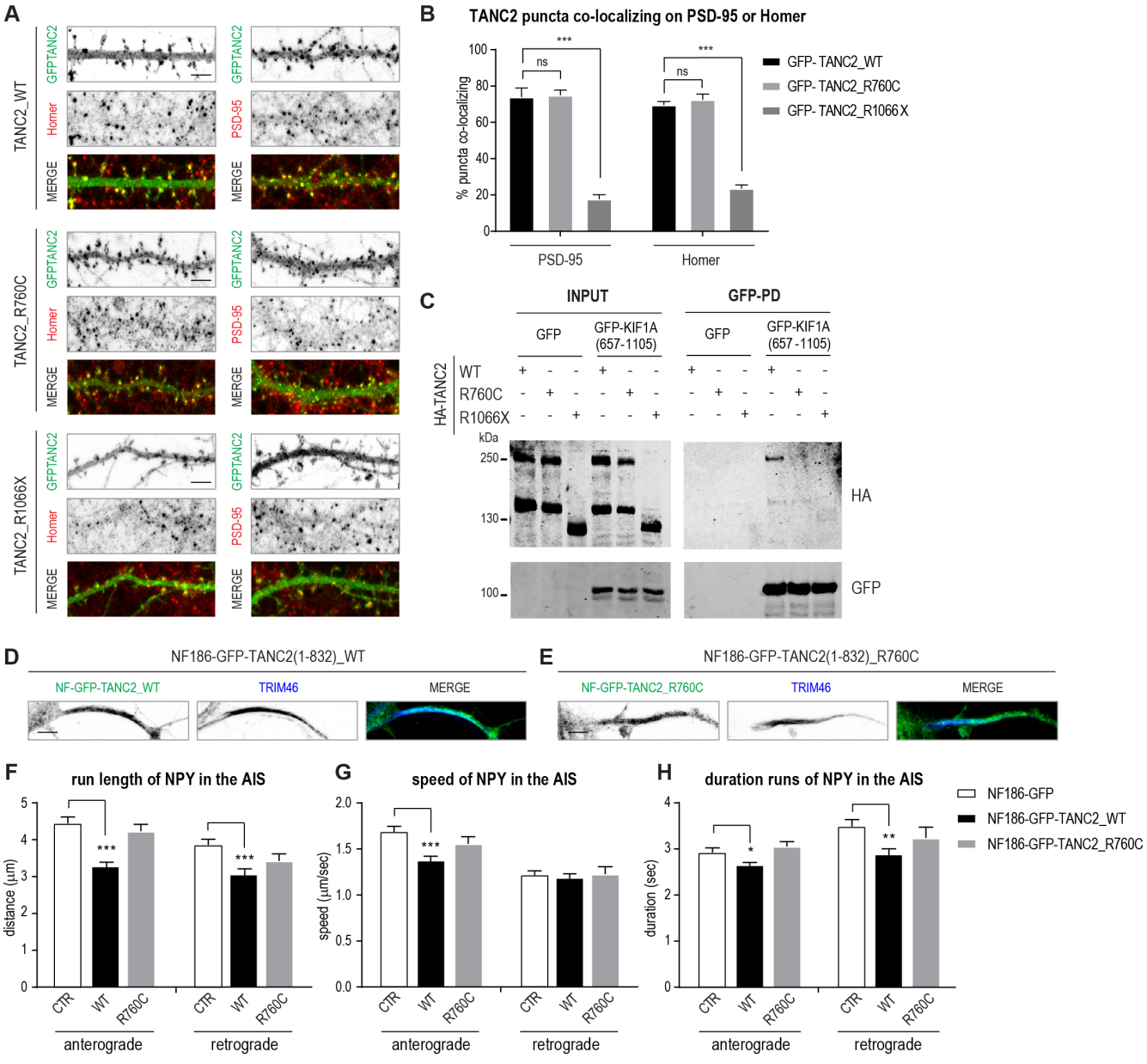

Figure S6. Related to Figure 7. TANC2 disease mutations affect KIF1A binding and DCV recruitment

(A) Representative dendritic protrusions of neurons (DIV14-17) expressing GFP-TANC2_WT, GFP-TANC2_R760C or GFP-TANC2_R1066X (green) and stained for the post-synaptic markers Homer or PSD-95 (red). Scale bar, 5μm.
(B) Quantifications corresponding to the percentage of GFP-TANC2 co-localizing puncta with endogenous Homer or PSD-95 shown in Figure S6A. The bars show mean ± s.e.m. (n=20-33 dendrites, ***P<0.001, t-test).
(C) Western blots of HA-TANC2_WT, HA-TANC_R760C and HA-TANC2_R1066X in AP experiments of bioGFP or bioGFP-KIF1A(657-1105) from co-transfected HEK293 cells.
(D-E) Zoom of the proximal axon in DIV11 hippocampal neurons transfected with NF186-GFP-TANC2(1-832)_WT (WT) (D) or NF186-GFP-TANC2(1-832)_R760C (R760C) (E) and stained for TRIM46 (blue). Scale bar, 5μm.
(F-H) Quantifications of average run length (F), speed (G) and run duration (H) of anterograde/retrograde transport of NPY-RFP vesicles in the AIS of neurons co-expressing NF186-GFP (CTR), NF186-GFP-TANC2(1-832)_WT (WT) or NF186-GFP-TANC2(1-832)_R760C (R760C). The bars show mean ± s.e.m. (n=37-40 neurons; n=202-412 vesicles; *P<0.05, t-test, **P<0.01, t-test, ***P<0.001, t-test).

SUPPLEMENTAL EXPERIMENTAL PROCEDURES

Animals

All experiments were approved by the DEC Dutch Animal Experiments Committee (Dier Experimenten Commisie), performed in line with institutional guidelines of Utrecht University and conducted in agreement with the Dutch law (Wet op de Dierproven, 1996) and European regulations (Directive 2010/63/EU). Female pregnant Wister rats were obtained from Janvier Laboratories. Upon delivery, rats were kept in a controlled 12h light-dark cycle with a temperature of 22°C and were given unrestricted access to food and water. The animals were housed with companions in transparent Plexiglas cages with wood-chip bedding and paper tissue for nest building and cage enrichment. Hippocampal neurons were obtained from embryos of both genders at E18 stage of development. None of the parameters analyzed in this study are reported to be affected by embryo gender. Pregnant female rats and embryos have not been involved in previous procedures.

Antibodies and reagents

The following primary and secondary antibodies were used in this study: Homer rabbit (SySy), PSD-95 mouse (NeuroMab), TRIM46 rabbit (van Beuningen et al., 2015),Tubα1a rabbit (Abcam), GFP rabbit (Abcam), MAP2 mouse (Sigma), MAP2 rabbit (Cell Signaling), mCherry mouse (Clontech), HA mouse (Covance), HA rabbit (Santa Cruz), FLAG mouse (Sigma), TANC1 rabbit (Abcam), TANC2 rabbit (Abcam), PanTANC (Han et al., 2010), and liprin-α1 (Spangler et al., 2013). Alexa405-, Alexa 488-, Alexa 568- and Alexa 594-conjugated secondary antibodies (Invitrogen). Other reagents used in this study include: jasplakinolide (2792, Tocris Bioscience), latrunculinB (SC-203318, Bioconnect), BAPTA-AM (SC-202488, Santa Cruz), bicuculline (Sigma), Streptavidin Dynabeads M-280 (Thermo Scientific), GFP-Trap® beads (ChromoTek), Calmodulin-Sepharose beads (Biovision), recombinant Calmodulin (C4874, Sigma).

Expression vectors and shRNA constructs

The following mammalian expression plasmids have been previously described: BirA coding vector and pebioGFP (van der Vaart et al., 2013), pGW1-GFP (Jaworski et al., 2009), pSuper vector (Brummelkamp et al., 2002), pGW2-MARCKS-GFP (Schatzle et al., 2011), pGW1-HA-liprin-α2, pGW1-GFP-liprin-α2, pGW1-GFP-liprin-α2(1-735), pGW1-GFP-liprin-α2(796-1257) and peBioGFP-liprin-α2 (Spangler et al., 2013), pGW1-HA-KIF1A (Kevenaar et al., 2016), pGW1-GFP-KIF1A (Lee et al., 2003), pGW2-NPY-GFP and pGW2-NPY-RFP (Schlager et al., 2010). pGW2-MARCKS-BFP was cloned by replacing GFP with cDNA encoding for BFP using BamHI and XbaI sites. pAAV-mCherry-Syt4, pAAV-mCherry-Syt11, pAAV-Syt4-phluorin, pAAV-Syt11-phluorin were kindly given us by Camin Dean. HA-CaM was generated by PCR on human-CAM1 cDNA kindly given us by Mike Boxem and cloned into a pGW2-HA linearized backbone using AscI and BamHI.

PebioGFP-KIF1A(657-1105), pebioGFP-KIF1A(393-881), pebioGFP-KIF1A(1105-1698), pebioGFP-KIF1A(950-1250), pebioGFP-KIF1A(657-1698) correspond to truncated versions of the KIF1A rat variant 2 (XM_003750741) and were kindly given us by Gary Banker; pebioGFP-KIF1A(691-752), (830-896), (986-1054) were produced by PCRs using pebioGFP-KIF1A(657-1105) as template and cloned using BamHI and XbaI sites; pebioGFP-KIF1A(657-1105)_5*Ala mutant was generated by gibson cloning (New England Biolabs) using 3 fragments: 1) gene blocks (IDT) to introduce 5 point mutations within the predicted CaM binding site (W714A, W716A, Y717A, F719A and L722A) (360b), 2) PCR product of pebioGFP-KIF1A657-1105 and 3) peBioGFP backbone digested with BamHI and AscI; pebioGFP-KIF1A657-1698_5*Ala mutant was generated with the same strategy but using the pebioGFP-KIF1A657-1698 as substrate for PCR of fragment 2; pGW1-HA-KIF1A(657-1105), pGW1-HA-KIF1A(657-1105)_5*Ala, pGW1-HA-KIF1A(657-1698), pGW1-HA-KIF1A(657-1698)_5*Ala were created using PCR based strategies and cloned into pGW1-HA vector using AscI and EcoRI sites; pGW1-GFP-KIF1A_5*Ala was created by Gibson cloning using 3 fragments: 1) pGW1-GFP-KIF1A digested with KpnI and BamHI 2-3) PCR products obtained using degenerated primers to introduce 5 point mutations in the CaM binding site; pGW1-HA-KIF1A(1-1105) was generated by PCR on pGW1-HA-KIF1A and cloned using AscI and EcoRI. pGW2-HA-TANC1 and pGW2-HA-TANC2 were generated using FLAG-TANC1 and FLAG-TANC2 (Han et al., 2010) as templates respectively and gene blocks (IDT) for the N-terminal part of the proteins and cloned into a pGW2-HA backbone using AscI and BamHI sites; peBioGFP-TANC2, b-actin-GFP-TANC2, b-actin-myc-tagRFP-TANC2 were generated using as template pGW2-HA-TANC2; b-actin-GFP-TANC2(1-832, 833-1227, 1228-1500, 1501-1900) were created by PCR strategies and cloned into b-actin-GFP vector using AscI and BamHI sites; pGW2-HA-TANC2_R760C and pGW2-HA-TANC2_R1066X were generated by Gibson cloning using pGW2-HA-TANC2_WT as template for PCRs and a pGW2-HA linearized backbone; b-actin-GFP-TANC2_R760C and b-actin-GFP-TANC2_ R1066X were generated by PCR based strategies using b-actin-GFP-TANC2 as backbone and pGW2-HA-TANC2_R760C and pGW2-HA-TANC2_R1066X as templates for PCR reactions. pGW1-NF186-GFP-TANC2(1-832)_WT and _R760C were produced by PCRs based strategies using b-actin-GFP-TANC2_WT or _R760C as templates and by cloning these PCRs products into a pGW1-NF186 (Kuijpers et al., 2016) backbone using AscI/XbaI sites.

The following shRNA sequences are used in this study: TANC2#1 (5'-CCTCAGTCAAGGGTCATAT), TANC2#2 (5'-GGAGCTGAAACCGAAATCT) and TANC2#3 (5'-GGCCAGTAAATACCAATCT) targeting rat TANC2 mRNA (XM_008768351.1) were designed using the siRNA selection program at the Whitehead Institute for Biomedical Research (jura.wi.mit.edu/bioc/siRNAext) (Yuan et al., 2004) and the complementary oligonucleotides were annealed and inserted

into a pSuper vector (Brummelkamp et al., 2002; Hoogenraad et al., 2005). ShRNA_KIF1A has been already described (Kevenaar et al., 2016) as well as shRNA_liprin-α2, shRNA_liprin-α3 (Spangler et al., 2013) and shRNA_cortactin (Jaworski et al., 2009). The control pSuper vector contains a scrambled sequence.

Primary hippocampal neuron cultures, transfections and drug treatments

Primary hippocampal cultures were prepared from embryonic day 18 rat brains. Cells were plated on coverslips coated with poly-L-lysine (30µg /ml) and laminin (2µg/ml) at a density of 100.000/well as previously described (Goslin and Banker, 1989; Kapitein et al., 2010). Hippocampal cultures were grown in Neurobasal medium (NB) supplemented with B27, 0.5 mM glutamine, 12.5 µM glutamate and penicillin/streptomycin.

Hippocampal neurons at DIV 11-14 / 14-17 were transfected using Lipofectamine 2000 (Invitrogen). Briefly, DNA (1.8 µg/well, for a 12 wells plate) was mixed with 3.3 µl of Lipofectamine 2000 in 200 µl NB, incubated for 30 min, and then added to the neurons in NB at 37°C in 5% CO2 for 45 min. Next, neurons were washed with NB and transferred in their original medium at 37°C in 5% CO2 for 2-3 days. 10 µM latrunculin B, 10 µM jasplakinolide, 10 µM BAPTA-AM or 40µM bicuculline were added to neuron cultures and fixed or imaged from 0 to 1h after addition.

Affinity Purification-Western blot (AP-WB) using biotin or GFP pull-down

Human Embryonic Kidney 293 cells (HEK293) cells were cultured in DMEM/Ham's F10 (50%/50%) containing 10% Fetal Calf Serum (FCS) and 1% penicillin/streptomycin at 37°C and 5% CO2. HEK293 cells were transfected with pe-Biotin-GFP constructs in combination with BirA or with GFP tagged constructs using polyethylenimine (PEI, Polysciences) according to the manufacturer instructions. Cells were lysed 48h later in lysis buffer (50mM TrisHCl (PH 7.4-7.8), 100mM NaCl, 0.5% TX-100, 5mM MgCl2, protease inhibitors (Roche)), centrifuged at 13.000 rpm for 15 min and the supernatants were incubated with either Streptavidin Dynabeads M-280 (Thermo Scientific) or GFP-trap beads (Chromotek) for 1h at 4°C. Beads were then separated using a magnet (Dynal, Invitrogen) and washed five times in washing buffer (20mM Tris HCl, 150mM KCl, 0.1% TritonX-100). Proteins were eluted from the beads by adding a 4x dilution of the sample buffer (8% SDS, 25% glycerol, 0.05M Tris pH 6.8, 400mM DTT and 40mg/l bromophenol blue). Samples were then boiled at 99ºC for 10 minutes before being analyzed by SDS PAGE. Proteins were transferred on nitrocellulose membranes (Millipore) using a semi-dry blotting system. Membranes were blocked with 3% BSA in PBS-T (0.1% Tween-20) and incubated with primary antibodies (overnight at 4°C) in 3% BSA PBS-T. IRdye680 or IRdye800-conjugated secondary antibodies (Li-Cor) were diluted 1:20.000 in 3%BSA-PBST and applied for 1h at RT. Blots were acquired using a LICOR Odyssey scanner at 680nm or 800nm. To quantify the relative amount of a specific co-precipitated protein, the intensity of each band was measured and then normalized to the intensities of the corresponding INPUT loading control band and to the intensity of the band relative to the purified bait protein. Quantifications were performed with Image J software (Universal Imaging Corporation).

Affinity Purification-Mass spectrometry (AP-MS) using biotin or GFP pull-down on rat brain extracts

Human Embryonic Kidney 293 cells (HEK293) cells were cultured in DMEM/Ham's F10 (50%/50%) containing 10% Fetal Calf Serum (FCS) and 1% penicillin/streptomycin at 37°C and 5% CO2. HEK293 cells were transfected with pe-Biotin-GFP constructs in combination with BirA or with GFP-constructs using polyethylenimine (PEI, Polysciences) according to

the manufacturer instructions. Cells were lysed 48h later in RIPA lysis buffer (50mM TrisHCl pH 7.4-7.8, 150mM NaCl, 1%Triton X-100, 0.1% SDS, 0.5% Sodium Deoxycholate and Protease inhibitors (Roche)), centrifuged at 13.000 rpm for 15 min and the supernatants were incubated for 1h at 4°C with either Streptavidin Dynabeads M-280 (Thermo Scientific) or GFP-trap beads (Chromotek), previously blocked in chicken egg albumin (Life Technologies). Beads were then separated using a magnet (Dynal, Invitrogen) washed twice in low salt washing buffer (20mM Tris-HCl pH 7.4-7.8, 100 mM KCl, 0.1% Triton X-100), followed by two washing steps in high salt wash buffer (20mM Tris-HCl pH 7.4-7.8, 500 mM KCl, 0.1% Triton X-100) and two final steps in low salt washing buffer (20mM Tris-HCl pH 7.4-7.8, 100 mM KCl, 0.1% Triton X-100) to remove binding proteins from HEK293 cells. Brains were obtained from female adult rats and homogenized in 10x volume/weight in tissue lysis buffer (50mM TrisHCl, 150mM NaCl, 0.1% SDS, 0.2% NP-40, and protease inhibitors). Brain lysates were centrifuged at 16,000 g for 15 min at 4°C and the supernatant was then incubated for 1h at 4°C with beads previously conjugated with either the biotinylated or the GFP-tagged proteins of interest. Beads were then separated using a magnet (Dynal; Invitrogen) and washed in normal washing buffer (20mM Tris HCl, 150mM KCl, 0.1% TritonX-100) for five times. For MS analysis, the beads were resuspended in 15 µl of Laemmli Sample buffer (Biorad), boiled at 99ºC for 10 minutes and supernatants were loaded on 4-12% Criterion XT Bis-Tris precast gel (Biorad). The gel was fixed with 40% methanol and 10% acetic acid and then stained for 1h using colloidal coomassie dye G-250 (Gel Code Blue Stain Reagent, Thermo Scientific). Each lane from the gel was cut in 3 slices, destained and digested using trypsin, as described in (Ekkebus et al., 2013). Briefly, each lane from the gel was cut into three pieces and placed in 0.5-ml tubes. Gel pieces were then washed with 250 µl of water, followed by 15 min dehydration in acetonitrile. Proteins were reduced (10 mM dithiothreitol, 1h at 56°C), dehydrated and alkylated (55 mM iodoacetamide, 1h in the dark). After two rounds of dehydration, trypsin (Promega) was added to the samples (20 µl of 0.1 mg/ml trypsin in 50 mM Ammoniumbicarbonate) and incubated overnight at 37°C. Peptides were extracted with ACN, dried down and reconstituted in 10% formic acid prior MS analysis.

***In vitro* Co-purification of KIF1A using sepharose CaM beads**

Equal amounts of lysates from HEK293 cells transfected with KIF1A(657-1105) or KIF1A(657-1105)5*Ala were incubated for 4h at 4°C with Calmodulin-Sepharose beads (Biovision) with increasing µM concentration of Ca^{2+} or EDTA. Beads were then washed with normal washing buffer (20mM Tris HCl, 150mM KCl, 0.1% TritonX-100) for 3 times by centrifuging them at 1500g for 3min. Proteins were eluted from the beads by adding a 4x dilution of the sample buffer (8% SDS, 25% glycerol, 0.05M Tris pH 6.8, 400mM DTT and 40mg/l bromophenol blue). Samples were then boiled at 99ºC for 10 minutes before being analyzed by SDS PAGE.

Immunoprecipitation on rat brain extracts

Rat brain extracts were obtained from female adult rats and homogenized in 10x volume/weight in tissue lysis buffer (50mM TrisHCl, 150mM NaCl, 0.1% SDS, 0.2% NP-40, and protease inhibitors). Brain lysates were centrifuged at 16.000 g for 15 min at 4°C and the supernatant was used for the immunoprecipitations. IPs were performed using Pierce Crosslink IP kit (Thermo Scientific) according to manufacturer recommended protocol. TANC1 rabbit (Abcam), TANC2 rabbit (Abcam), PanTANC (Han et al., 2010) were the antibodies used for the IP experiments.

Mass spectrometry analysis

All samples were analyzed on an ETD enabled LTQ-Orbitrap Elite coupled to Proxeon EASY-nLC 1000 (Thermo Fisher Scientific, Odense, Denmark) or on an Orbitrap Q-Exactive mass spectrometer (Thermo Fisher Scientific, Bremen, Germany) coupled to an Agilent 1290 Infinity LC (Agilent Technologies). Peptides were loaded onto a trap column (Reprosil pur C18, Dr. Maisch, 100 µm x 2 cm, 3 µm; constructed in-house) with solvent A (0.1% formic acid in water) at a maximum pressure of 800 bar and chromatographically separated over the analytical column (Poroshell 120 EC C18, Agilent Technologies, 50 µm x 50 cm, 2.7 µm) using 90 min linear gradient from 7-30% solvent B (0.1% formic acid in acetonitrile) at a flow rate of 150 nL/min. The mass spectrometers were used in a data-dependent mode, which automatically switched between MS and MS/MS. After a survey scan from 350-1500 m/z the 10 or 20 most abundant peptides were subjected to either CID or HCD fragmentation depending on the MS-spectrometer used. MS spectra were acquired in high-resolution mode (R > 30,000), whereas MS2 was in high-sensitivity mode (R > 15,000). For data analysis, raw files were processed using Proteome Discoverer 1.4 (version 1.4.1.14, Thermo Scientific, Bremen, Germany). Database search was performed using the Uniprot rat database and Mascot (version 2.5.1, Matrix Science, UK) as the search engine. Carbamidomethylation of cysteines was set as a fixed modification and oxidation of methionine was set as a variable modification. Trypsin was set as cleavage specificity, allowing a maximum of 2 missed cleavages. Data filtering was performed using a percolator (Kall et al., 2007), resulting in 1% false discovery rate (FDR). Additional filters were search engine rank 1 and mascot ion score >20. The mass spectrometry proteomics data have been deposited to the ProteomeXchange Consortium via the PRIDE (Vizcaino et al., 2016) partner repository with the dataset identifier PXD010080.

Cross linking Mass Spectrometry (XL-MS)

For crosslinking experiment, the beads with affinity-precipitated proteins were incubated with 2 mM disuccinimidyl sulfoxide (DSSO; ThermoFischer Scientific) crosslinker for 1h at room temperature (Kao et al., 2011). The crosslinking reaction was quenched with 20 mM Tris-HCl for 20 min at room temperature. On-beads crosslinked proteins were denatured with 2 mM Urea, reduced with 4 mM dithiothreithol at 56^0C for 30 min and then alkylated with 8mM iodoacetamide for 30 min in the dark. Proteins were partially digested using trypsin (Promega) at 37^0C for 2h. The supernatant was removed from the beads, fresh aliquot of trypsin was added and further digested overnight at 37^0C. Crosslinked protein digests were subsequently desalted and enriched with Strong Cation Exchange (SCX) Stage Tips. Obtained fractions were dried and stored at -80^0C for further use.

Crosslinked peptide mixtures were reconstituted in DMSO/FA/HOH 5%/10%/85% (v/v/v) mixture and analyzed on an Orbitrap Fusion Lumos (ThermoFisher Scientific) coupled online to an Agilent UPLC 1290 system (Agilent Technologies). Crosslinked peptide digest was trapped on a pre-column (Reprosil pur C18, Dr. Maisch, 100 µm x 2 cm, 3 µm; constructed in-house) for 10 min with buffer A (0.1% formic acid) and separated on an analytical column (Poroshell 120 EC C18, Agilent Technologies, 50 µm x 50 cm, 2.7 µm) over 65 min with a linear gradient from 10% to 40% B (B: 0.1% formic acid, 80% acetonitrile). MS data acquisition was performed using MS2_MS3 acquisition strategy: at the MS^1 level survey scan was recorded in Orbitrap (OT) at 60.000 resolution. For selected precursors collisional-induced dissociation (CID) was applied and signature peaks for the crosslinkers were recorded at 30000 resolution. Fragments exhibiting patterns associated to the DSSO cleavable crosslinker were further subjected to low-resolution MS^3 scan in the ion trap (IT) (Kao et al., 2011;

Liu et al., 2017). Raw data files were processed in Proteome Discoverer 2.2 with in-house developed nodes for crosslink analysis (Liu et al., 2015). The mass spectrometry proteomics data have been deposited to the ProteomeXchange Consortium via the PRIDE (Vizcaino et al., 2016) partner repository with the dataset identifier PXD010080.

Bioinformatic analysis

Gene ontology (GO) classification was obtained via PANTER (Mi et al., 2005). Statistical assessment of the AP-MS data was performed based on spectral counts using the SAINT (Significance Analysis of INTeractions, version 2.3.2) algorithm (Choi et al., 2011) . The SAINT parameters were set as follows: nburn=2000, niter=20.000, lowmode=0, minfold=0, and norm=1. Bait proteins with a SAINT probability score >0.90 were considered putative protein interaction partners.

Immunofluorescent staining

Neurons were fixed for 10 min with 4% formaldehyde/4% sucrose in phosphate-buffered saline (PBS) at room temperature. After fixation cells were washed three times for 10 min in PBS, incubated for 10 min with permeabilization buffer (0.25% TritonX-100 in PBS) and then blocked for 1h with blocking buffer (2% BSA, 2% Glycin, 0.2% Gelatin, 50mM NH_4Cl, in PBS). Neurons were then incubated with primary antibodies diluted in blocking buffer overnight at 4°C, washed three times in PBS for 10 min and then incubated with Alexa-conjugated secondary antibodies in blocking buffer for 1h at room temperature. Neurons were then washed 3 times for 5 min in PBS at room temperature and subsequently mounted on slides in Vectashield mounting medium (Vector Laboratories). Confocal images were acquired using a LSM 700 confocal laser-scanning microscope (Zeiss) with a 40×1.3 N.A or 63×1.4 N.A. oil objective (Zeiss). Each image was a z-series of ~7-10 images, each averaged 2 times and was chosen to cover the entire region of interest from top to bottom. The resulting z-stack was ‘‘flattened’’ into a single image using maximum projection. Images were not further processed and were of similar high quality to the original single planes. The confocal settings were kept the same for all scans when fluorescence intensity was compared. Morphometric analysis, quantification, and co-localization were performed using ImageJ software (Universal Imaging Corporation). See for details the methods section: Image analysis and quantification.

Image analysis and quantification

Quantification of TANC2 knockdown efficiency by immunostaining in cultured hippocampal neurons

Efficiency of TANC2 shRNAs knock down was verified by immunostaining of endogenous TANC2 protein in hippocampal neurons co-transfected at DIV11 with 0.45 µg/well GFP and 1.35 µg/well of different TANC2-shRNAs or a mixture of all of them, and fixed 3 days later (DIV14). TANC2 staining (rabbit polyclonal anti-TANC2 antibody, Abcam) was measured both in the soma and in the neurites of GFP positive neurons and was compared to TANC2 corresponding staining in GFP negative surrounding cells within the same image. Images were acquired using a LSM 700 confocal laser-scanning microscope (Zeiss) using a plan-apo 40×1.3 N.A with the same settings and the exposure time and taking series of stacks from the bottom to the top. Maximum intensity projections were created using ZEN 2014 software (Zeiss) and later used for the analyses. ImageJ was used to manually draw specific regions of interest (ROI) located in the soma and in at least three primary neurites. From the ROIs the mean intensity was then measured. To prevent selection bias during quantification, the regions of interest in TANC2-KD neurons were selected in one channel (GFP) and blindly quantified in the other channel (TANC2 intensity). Intensities were measured in segments of approximately the same size, both in GFP positives and GFP

negatives neurons. To remove the background signal, the intensity near the selected areas (same segment size) was measured and subtracted to the measured intensities within the same image. Normalized intensities were averaged over multiple cells and a statistical analysis was performed with student's t test assuming a two-tailed and unequal variation.

Dendritic protrusions analysis

To highlight protrusions morphology, neurons were transfected at DIV11 and fixed at DIV14 using MARCKS-GFP as an unbiased cell-fill in combination with our constructs of interest up to a maximum of 1.8 µg of total DNA/well. Confocal images were acquired using a LSM700 confocal laser-scanning microscope (Zeiss) with a 63x oil objective. The confocal laser intensity settings were optimized for each neuron. The resulting z-stack used for the spine counting was a single image processed by using the maximum projection function of ZEN2014 software (Zeiss). Images were not further processed and were of similar high quality to the original single planes. Morphological analysis and quantification were performed using ImageJ. For each neuron three dendrites were selected and boxes of 20 µm of length were placed 20 µm from the soma. Within these boxes the number of mushroom, filopodia-like and stubby spines were counted manually by using the Cell Counter plugin.

Quantification of fluorescent intensity in neurons

For the quantification of fluorescent intensity, images were acquired on a LSM700 confocal microscope (Zeiss) using a plan-apo 40×1.3 N.A objective and intensity of signals in the cell body and neurites were measured using ImageJ software. Because neurites often crossed several z planes, series of stacks were taken from the bottom to the top and the ZEN 2014 software (Zeiss) was used to generate image projections for quantitative analyses. To prevent selection bias during quantification, the neurites segments were selected in one channel (GFP, RFP or BFP to visualize neuronal morphology) and quantified in the other channel. To control for background signals the intensity of an area of the same size was measured near the selected neuron and the measured random fluorescent intensity was subtracted in these images. Intensities were averaged over multiple cells and normalized.

Quantification of KIF1A and DCV distribution in dendritic spines

To highlight protrusions morphology, neurons were transfected at DIV14 and fixed at DIV17 using MARCKS-BFP as an unbiased cell-fill in combination with our constructs of interest (KIF1A, NPY, Syt4) up to a maximum of 1.8 ug of total DNA/well. Confocal images were acquired using a LSM700 confocal laser-scanning microscope (Zeiss) with a 63x oil objective. The confocal laser intensity settings were optimized for each neuron. The resulting z-stack used for the counting was a single image processed with the maximum projection function of ZEN2014 software (Zeiss). To prevent selection bias during quantification, the selected dendritic fragments were selected in the BFP channel. For each neuron three dendrites were selected and boxes of 20 µm of length were placed approximately 20 µm from the soma; then KIF1A, NPY or Syt4 puncta were counted in each single spine along 20 µm as well as in the dendritic shaft. Ratios of puncta spines/shaft were then normalized for the total number of spines along 20 µm to correct for different spines densities in different conditions.

Live cell imaging and imaging processing

Live-cell imaging experiments were performed in an inverted microscope Nikon Eclipse Ti-E (Nikon), equipped with a Plan Apo VC 100x NA 1.40 oil or a 60x NA 1.40 oil, a Yokogawa CSU-X1-A1 spinning disk confocal unit (Roper Scientific), a Photometrics Evolve 512 EMCCD camera (Roper Scientific) and an incubation chamber (Tokai Hit) mounted on a

motorized XYZ stage (Applied Scientific Instrumentation) which were all controlled using MetaMorph (Molecular Devices) software. Neurites that were in close proximity to the soma were selected for imaging.

Imaging and analysis of motility of NPY and Syt4 motility

Time-lapses were acquired with 1 sec intervals for 5min, later analyzed for motility of vesicles. Motility was analyzed by pseudocoloring 1st frame in green and 10th frame in red. Merging those frames revealed vesicles non-colocalizing (motile), partially and fully co-localizing (immotile).

Imaging and analysis of motility of KIF1A, NPY, Syt4 upon BAPTA treatment

For motility analyses, time-lapses were acquired with 1 sec intervals for 5min, later analyzed for motility of vesicles. BAPTA-AM or DMSO were pipetted to the sample at a final concentration of 10uM. Motility was analyzed by pseudocoloring 1st frame in green and 10th frame in red. Merging those frames revealed vesicles non-colocalizing (motile), partially and fully co-localizing (immotile).

Imaging and analysis of motility of KIF1A, NPY upon bicuculline treatment

Time lapse images in GFP and RFP channels were carried at 1 frame per second intervals, for 10 minutes before addition of DMSO or bicuculline. Treatments were pipetted to the sample and imaging of the same field of view was carried for another 10 minutes. To analyze the mobility of KIF1A and NPY along neurites, 3-5 neurite segments were selected from each field of view. The same segments were selected from the time lapse taken before and after addition of treatments. Only segments that were of at least 15µm in length and with minimal crossings by other neurites were selected for kymographs based analysis. Using Fiji software, segments were traced with a line-ROI and kymographs were separately created using the Multi Kymograph plugin. The number of KIF1A and co-localized, mobile KIF1A and NPY traces of each kymograph were manually counted.

Imaging and analysis of motility of KIF1A, NPY, Syt4 in combination with the scaffolding proteins liprin-α2 and TANC2.

Time-lapses were acquired with 1 sec intervals for 5min, in neurons (DIV14, DIV17) co-transfected with GFP- or RFP-tagged TANC2 or liprin-α2 in combination with GFP-, RFP- or mCherry-tagged KIF1A, NPY or Syt4. To analyze the mobility of DCVs along neurites, 3-5 neurite segments were selected from each field of view. To calculate the percentage of DCV pausing within or outside static TANC2/liprin-α2 spots, kymographs were obtained and subsequently analyzed. NPY was used as marker for DCVs. NPY pausing was calculated as percentage of the ratio of NPY pauses at TANC2/liprin-α2 positive clusters on the total amount of NPY pauses.

Imaging and analysis of NPY motility in the axon initial segment (AIS) of neurons transfected with Neurofascin-TANC2 fusion proteins.

Time lapse images in GFP and RFP channels were carried at 5 frames per second intervals, for 50 seconds. Neurons (DIV11) were co-transfected with NPY-RFP in combination with NF186-GFP or NF186-GFP-TANC2(1-832)_WT or NF186-GFP-TANC2(1-832)_R760C. The AIS of transfected neurons was clearly detectable in the green channel because of the accumulation of NF186 and NF186 chimeric proteins in this region. After the AIS was visualized in green, the RFP channel was used for the imaging of NPY vesicles in the same region. For the analysis, a z-projection of the average intensity of the movie was made and subtracted from the original movie to background fluorescence and non-moving particles. A line of approximately 10-20µm in each AIS was drawn. Kymographs of these lines were then created using KymoResliceWide plugin. Clearly visible anterograde and retrograde traces were traced on the kymos by drawing straight lines. Length and angle of the lines were measured and used to calculate velocity, run length and duration.

SUPPLEMENTAL REFERENCES

- Brummelkamp, T.R., Bernards, R., and Agami, R. (2002). Stable suppression of tumorigenicity by virus-mediated RNA interference. Cancer Cell 2, 243-247.
- Choi, H., Larsen, B., Lin, Z.Y., Breitkreutz, A., Mellacheruvu, D., Fermin, D., Qin, Z.S., Tyers, M., Gingras, A.C., and Nesvizhskii, A.I. (2011). SAINT: probabilistic scoring of affinity purification-mass spectrometry data. Nat Methods 8, 70-73.
- Ekkebus, R., van Kasteren, S.I., Kulathu, Y., Scholten, A., Berlin, I., Geurink, P.P., de Jong, A., Goerdayal, S., Neefjes, J., Heck, A.J.*, et al.* (2013). On terminal alkynes that can react with active-site cysteine nucleophiles in proteases. J Am Chem Soc 135, 2867-2870.
- Goslin, K., and Banker, G. (1989). Experimental observations on the development of polarity by hippocampal neurons in culture. J Cell Biol 108, 1507-1516.
- Han, S., Nam, J., Li, Y., Kim, S., Cho, S.H., Cho, Y.S., Choi, S.Y., Choi, J., Han, K., Kim, Y.*, et al.* (2010). Regulation of dendritic spines, spatial memory, and embryonic development by the TANC family of PSD-95-interacting proteins. J Neurosci 30, 15102-15112.
- Hoogenraad, C.C., Milstein, A.D., Ethell, I.M., Henkemeyer, M., and Sheng, M. (2005). GRIP1 controls dendrite morphogenesis by regulating EphB receptor trafficking. Nat Neurosci 8, 906-915.
- Jaworski, J., Kapitein, L.C., Gouveia, S.M., Dortland, B.R., Wulf, P.S., Grigoriev, I., Camera, P., Spangler, S.A., Di Stefano, P., Demmers, J.*, et al.* (2009). Dynamic microtubules regulate dendritic spine morphology and synaptic plasticity. Neuron 61, 85-100.
- Kall, L., Canterbury, J.D., Weston, J., Noble, W.S., and MacCoss, M.J. (2007). Semi-supervised learning for peptide identification from shotgun proteomics datasets. Nat Methods 4, 923-925.
- Kao, A., Chiu, C.L., Vellucci, D., Yang, Y., Patel, V.R., Guan, S., Randall, A., Baldi, P., Rychnovsky, S.D., and Huang, L. (2011). Development of a novel cross-linking strategy for fast and accurate identification of cross-linked peptides of protein complexes. Mol Cell Proteomics 10, M110 002212.
- Kapitein, L.C., Yau, K.W., and Hoogenraad, C.C. (2010). Microtubule dynamics in dendritic spines. Methods Cell Biol 97, 111-132.
- Kevenaar, J.T., Bianchi, S., van Spronsen, M., Olieric, N., Lipka, J., Frias, C.P., Mikhaylova, M., Harterink, M., Keijzer, N., Wulf, P.S.*, et al.* (2016). Kinesin-Binding Protein Controls Microtubule Dynamics and Cargo Trafficking by Regulating Kinesin Motor Activity. Curr Biol 26, 849-861.
- Kuijpers, M., van de Willige, D., Freal, A., Chazeau, A., Franker, M.A., Hofenk, J., Rodrigues, R.J., Kapitein, L.C., Akhmanova, A., Jaarsma, D., and Hoogenraad, C.C. (2016). Dynein Regulator NDEL1 Controls Polarized Cargo Transport at the Axon Initial Segment. Neuron 89, 461-471.

- Lee, J.R., Shin, H., Ko, J., Choi, J., Lee, H., and Kim, E. (2003). Characterization of the movement of the kinesin motor KIF1A in living cultured neurons. J Biol Chem 278, 2624-2629.
- Liu, F., Lossl, P., Scheltema, R., Viner, R., and Heck, A.J.R. (2017). Optimized fragmentation schemes and data analysis strategies for proteome-wide cross-link identification. Nat Commun 8, 15473.
- Liu, F., Rijkers, D.T., Post, H., and Heck, A.J. (2015). Proteome-wide profiling of protein assemblies by cross-linking mass spectrometry. Nat Methods 12, 1179-1184.
- Mi, H., Lazareva-Ulitsky, B., Loo, R., Kejariwal, A., Vandergriff, J., Rabkin, S., Guo, N., Muruganujan, A., Doremieux, O., Campbell, M.J.*, et al.* (2005). The PANTHER database of protein families, subfamilies, functions and pathways. Nucleic Acids Res 33, D284-288.
- Schatzle, P., Ster, J., Verbich, D., McKinney, R.A., Gerber, U., Sonderegger, P., and Mateos, J.M. (2011). Rapid and reversible formation of spine head filopodia in response to muscarinic receptor activation in CA1 pyramidal cells. J Physiol 589, 4353-4364.
- Schlager, M.A., Kapitein, L.C., Grigoriev, I., Burzynski, G.M., Wulf, P.S., Keijzer, N., de Graaff, E., Fukuda, M., Shepherd, I.T., Akhmanova, A., and Hoogenraad, C.C. (2010). Pericentrosomal targeting of Rab6 secretory vesicles by Bicaudal-D-related protein 1 (BICDR-1) regulates neuritogenesis. EMBO J 29, 1637-1651.
- Spangler, S.A., Schmitz, S.K., Kevenaar, J.T., de Graaff, E., de Wit, H., Demmers, J., Toonen, R.F., and Hoogenraad, C.C. (2013). Liprin-alpha2 promotes the presynaptic recruitment and turnover of RIM1/CASK to facilitate synaptic transmission. J Cell Biol 201, 915-928.
- van Beuningen, S.F.B., Will, L., Harterink, M., Chazeau, A., van Battum, E.Y., Frias, C.P., Franker, M.A.M., Katrukha, E.A., Stucchi, R., Vocking, K.*, et al.* (2015). TRIM46 Controls Neuronal Polarity and Axon Specification by Driving the Formation of Parallel Microtubule Arrays. Neuron 88, 1208-1226.
- van der Vaart, B., van Riel, W.E., Doodhi, H., Kevenaar, J.T., Katrukha, E.A., Gumy, L., Bouchet, B.P., Grigoriev, I., Spangler, S.A., Yu, K.L.*, et al.* (2013). CFEOM1-associated kinesin KIF21A is a cortical microtubule growth inhibitor. Dev Cell 27, 145-160.
- Vizcaino, J.A., Csordas, A., Del-Toro, N., Dianes, J.A., Griss, J., Lavidas, I., Mayer, G., Perez-Riverol, Y., Reisinger, F., Ternent, T.*, et al.* (2016). 2016 update of the PRIDE database and its related tools. Nucleic Acids Res 44, 11033.
- Yuan, B., Latek, R., Hossbach, M., Tuschl, T., and Lewitter, F. (2004). siRNA Selection Server: an automated siRNA oligonucleotide prediction server. Nucleic Acids Res 32, W130-134.